Materials and Design 57 (2014) 135–145

Contents lists available at ScienceDirect

Materials and Design

journal homepage: www.elsevier.com/locate/matdes

New approaches to detect the onset of localised necking in sheets under through-thickness strain gradients

A.J. Martínez-Donaire, F.J. García-Lomas, C. Vallellano *

Group of Manufacturing Processes, Department of Mechanical and Manufacturing Engineering, University of Sevilla, Camino de los Descubrimientos s/n, 41092, Sevilla, Spain

ARTICLE INFO

Article history:
Received 10 October 2013
Accepted 4 January 2014
Available online 9 January 2014

Keywords:
Forming limit strain
Necking detection
Strain gradient
Time-dependent method
Time-position-dependent method

ABSTRACT

The standard ISO 12004-2:2008 provides a position-dependent methodology to estimate the limit strains in Nakazima- and Marciniak-type tests. However, this method is not applicable, at least in its current formulation, when there are significant strain gradients across the sheet thickness, such as when using relatively small punch radii or in stretch-bending operations very commonly in industrial practice. This paper analyses two physically-based methodologies, a time-dependent method and a time-position-dependent method (called here *flat-valley method*), to detect the onset of necking and to evaluate the limit strains under significant strain gradients through the sheet thickness. The digital image correlation (DIC) technique is used to compute the displacement and strain evolutions at the outer surface of the tested specimens using the commercial software ARAMIS®. A detailed analysis and validation of both methodologies, and comparison with other local methods recently published in the literature, are carried out in the light of a series of Nakazima tests and stretch-bending tests for different cylindrical punch radii in AA7075-O.

1. Introduction

The forming limit curve at necking (FLC) is one of the most widely used tools for evaluating sheet metal formability at the industrial level. This curve represents the maximum values of the principal strains (for the major strain ε_1 versus the minor strain ε_2) for the onset of localised necking in a sheet subjected to different "proportional" strain ratios. In this way, a boundary is established between strain states that facilitate sheet forming and those that produce sheet failure.

Both theoretical and experimental methods are being used in practice for the identification of the FLC. Within the theoretical framework, the pioneering work of Hill [1] postulated a criterion for the localised necking under plane stress conditions, in which the neck forms along the zero extension direction. This criterion was suitable for obtaining the left-hand side of the FLC. For the right-hand side, Swift [2] suggested that instability occurs when the principal stresses attain their maximum and predicted the critical strains for diffuse necking. But, perhaps, the most widely used analytical tool is the Marciniak–Kuczynski (M–K) model [3]. This is based on the assumption that necking occurs due to initial imperfections. In biaxial stretching, the onset of necking is associated with the establishment of a localised plane strain state at imperfections perpendicular to the major strain direction. Later, Hutchinson and Neale [4] improved the model to cover the whole range of the FLC. More recently, Eyckens et al. [5,6] have extended the M–K model to include Through-Thickness Shear (TTS) for both isotropic and anisotropic metal sheets. They claimed that formability seems to increase by TTS, this being a parameter to be explored in sheet forming processes in which sliding contact with friction between the punch and the sheet occurs, e.g. in incremental sheet forming.

A number of theoretical modelling based on the continuum plasticity have been reviewed by Zadpoor et al. [7]. They compared four different approaches for necking and fracture to predict the failure of the high strength aluminium alloy 2024-T3. The influence of the through-the-thickness strain gradient in postponing the onset of necking has been discussed by Zadpoor et al. [8] for 2024-T3 and 7075-T6 sheets. Zhang et al. [9] provided an approach to model the localised necking in anisotropic sheet metals to construct the FLC. Based on the plastic instability and uses Swift's diffuse necking and Hill's localised necking concepts, Firat [10] implemented two numerical models into Ls-Dyna to predict the FLC of a high-strength dual-phase steel using in-plane proportional loadings.

Although many efforts have been made to develop theoretical models to predict the FLC, its experimental determination is unavoidable to calibrate or validate these models. Furthermore, in many practical cases, the accurate obtaining of the FLC is mandatory to provide reliable results. The main difficulty is the precise detection of the onset of necking and the measurement of the sheet strain at this point. No standardised methodologies were available until the end of 2008; consequently, different experimental

* Corresponding author. Tel.: +34 954 487311.
E-mail address: carpofor@us.es (A.J. Martínez-Donaire).

http://dx.doi.org/10.1016/j.matdes.2014.01.012
0261-3069/

techniques have been used historically to determine the limit strains at the onset of necking.

The Bragard method [11,12] is one of the most traditional schemes for determining the strain at the onset of necking. Briefly, the method evaluates the distribution of the major strain along various sections perpendicular to the crack in the fractured specimen. The strain can be evaluated by manually measuring a pre-engraved grid pattern on the sheet or using recent techniques based on three-dimensional digital image correlation (DIC) [13]. The measured major strain distribution (ε_1) is fit, generally with a parabola or an inverse parabola, for each section of the sheet. The limit strain for necking in each section corresponds to the maximum value of the fitting function. Another classic method analyses the principal strain-paths using a ε_1–ε_2 diagram. The experimental observation shows the development of a local plane strain state at the onset of localised necking, independent of the global strain state applied to the sheet. That is, the initiation of necking is associated with an abrupt change in the slope of the ε_1–ε_2 curve because of the local plane strain conditions. Unlike the Bragard method, the strains have to be continuously evaluated during the sheet-forming process in this method. A detailed analysis of these criteria and other representative criteria to estimate the forming limits can be found in the literature [14,15].

Various techniques and principles from the aforementioned methodologies have been appropriated in the ISO standard 12004-2:2008, "Metallic materials – Sheet and strip – Determination of forming limit curves in laboratory" [16]. The standard aims to define specific test conditions and a unified evaluation procedure to reduce the dispersion between the FLC calculations from different laboratories. The current procedure is a position-dependent methodology in which the principal strain distributions are analysed for sections perpendicular to the crack immediately before the appearance of fracture. The procedure is called a position-dependent methodology because the onset of necking is estimated by analysing a single and unique instant in the process. A detailed analysis of the foundations and justification of the ISO 12004-2:2008 methodology has been given by Hotz and Timm [17]. The main steps in the practical application of ISO method have been discussed by Martínez-Donaire et al. [18,19].

Optical techniques and image analysis are being increasingly and extensively used to measure the strains automatically over the entire sample surface for the whole duration of the test. The innate ability to have the strain data continuously throughout the test using these techniques, allowed to explore and to formulate time-dependent methods for the FLC determination, as alternative to the position-dependent methodologies. Some of these methods were developed by Geiger and Merklein [20], Situ et al. [21–23], Eberle et al. [24], Feldmann et al. [25], Volk and Hora [26], Merklein et al. [27], Li et al. [28] and Hotz et al. [29], among others.

In Geiger and Merklein's method [20], the onset of necking is related to the appearance of a load instability in a region where the ε_1 distribution and its spatial gradient differs significantly from the rest of the sheet. The limit strains are estimated at the boundary of this region of instability. More recently, Merklein et al. [27] formulated a criterion involving the major strain rates ($\dot{\varepsilon}_1$) in regions far from and near to the failure region. The onset of necking is identified by applying a regression methodology that the authors previously developed [30].

Situ et al. [21–23] developed a method to analyse the temporal evolution of ε_1 and its first and second time derivatives (referred to as the strain rate and the strain acceleration, respectively) at a point in the fracture region. The onset of localised necking occurs at the instant at which an inflexion point is observed in the first time derivative of ε_1 (the strain rate, $\dot{\varepsilon}_1$), or equivalently, when the second derivative of ε_1 (the strain acceleration, $\ddot{\varepsilon}_1$) reaches a maximum. The authors considered that the reduction in ε_1 from a maximum value to zero represented the strain localisation process.

Feldmann et al. [25] developed an automated algorithm to determine the FLC, which has already implemented in the commercial software Autogrid. This method analyses the time evolution of the difference in the ε_1 strain increments (which are similar to the strain rates) between the most strained point in the failure region and adjacent points. The onset of the plastic instability and the limit strains were identified from the correlation coefficient for the linear fit of the different sections. Based on the previous work by Eberle et al. [24], Volk and Hora [26] proposed a temporal analysis of the thickness strain, ε_3, and of its first derivative (the thickness strain rate, $\dot{\varepsilon}_3$) along a section perpendicular to the failure region. Two straight lines were fitted along the representative thinning rate evolution, one through the stable deformation stages and the other through the last stages just before specimen failure. The authors hypothesised that the intersection of these lines defined the onset of the plastic instability. Li et al. [28] proposed to analyse the strain history and its first derivative with respect to image number from DIC at the most strained point on the specimen surface before fracture. The onset of diffuse necking was associated with the start of a rapid increase in the axial strain rate, which indicates the instability. The localised necking was identified at those points which started to lose information in the DIC postprocessing output. Hotz et al. [29] presented a comparison of four different time-dependent algorithms: a modification of the method by Volk and Hora [26], called here linear best fit; the one by Merklein et al. [27], referred to as correlation coefficient, and two methods proposed by the authors named gliding correlation coefficient and gliding difference of mean to median. Their predicted FLCs were compared with the ISO standard 12004-2:2008 [16]. It was observed that the FLCs obtained using these time-dependent methods showed values slightly greater than the FLC determined according to ISO.

Despite the plethora of existing techniques for determining the FLC, no method is universally accepted. Almost all of these methods were developed and optimised using Marciniak- and/or Nakazima-type tests, for which the curvature of the punches is zero or sufficiently small. In these cases, although slight differences in limit strains between both type of tests are expected, see for instance Leppin et al. [31], the bending effects are almost negligible in comparison with the one induced in stretch-bending tests. For this reason, many of these methods, including the ISO 12004-2:2008 standard [16], should not be applied to practical industrial applications in which strain gradient are relevant, e.g., operations with small-radii punches, corner radii in forming dies, etc.

The effect of bending on sheet formability was first clearly shown by Ghosh and Hecker [32] and later by Charpentier [33]. These studies showed the effect of the punch radius on the FLCs. Thus, the FLCs obtained by using hemispherical or elliptical punches (i.e., for out-of-plane tests), were consistently situated above FLCs that were determined under uniform strain conditions (i.e., Marciniak in-plane tests). Some authors consider the increase in forming limit strains to be a beneficial effect of the strain gradient across the thickness [34–40].

Kitting et al. [41] used a local criterion to estimate the forming limits in stretch-bending tests. In this formulation, the region where necking occurs is estimated using the strain rates in the final stages before failure along a section perpendicular to the fracture line. The limit strain is then defined as the average of the maximum strains at the boundaries of the necking region. The following sections show that this analysis, which can be acceptable when bending is small, can be inaccurate for very small punch radii.

Nowadays, there is no commonly accepted criterion for the assessment of the limit strains when bending effects are important. This paper analyses two physically-based methodologies to detect the onset of necking and to estimate the limit strains under

significant strain gradients through the sheet thickness. The first one is a time-dependent method recently outlined by the authors [18,19], which is here discussed and validated in detail and its physical basis is linked to the experimental observation. The second one, a time-position dependent method, referred to here as "flat-valley method", is based on direct visualisation and analysis of displacements at the outer sheet surface during necking development.

A series of Nakazima tests under different strain paths and stretch-bending tests, using cylindrical punches ranging from 20 to 5 mm diameter, are performed on aluminium alloy 7075-O sheets of 1.6 mm thickness. The digital image correlation (DIC) technique is used to compute the displacement and strain evolutions at the outer surface of the tested specimens using the commercial software ARAMIS®. A detailed analysis and validation of both methodologies, and comparison with other local methods recently published in the literature, are carried out in the light of the experimental results.

2. Time-dependent methodology to detect necking

Localised necking can be physically identified as an unstable local reduction in the sheet thickness in a region with a size of the order of the sheet thickness. Before the onset of necking, the sheet strain depends on the geometry of the forming tools and the sheet geometry. However, after the necking process begins, all the strain in the sheet becomes concentrated in this region. The strain rate in the material outside the necking zone decreases gradually until it finally vanishes.

Fig. 1 (top) illustrates the time evolution of the major strain in a stretch-bending test (using a cylindrical punch of Ø10mm) along a section perpendicular to the failure region. At the very beginning of the test, the strain profile uniformly increases with time in the whole section under consideration, showing a slightly dome-shaped geometry due to the punch radius. However, after a certain instant, the strain begins to concentrate within a highly localised band and the deformation raises up very quickly. In fact, two well-differentiated behaviours can be observed in Fig. 1 (bottom), which shows the time evolution of ε_1 at various aligned points from the previous section. The strain level of some points (B and C) increases monotonically until fracture, while other points (A, D and E) cease to strain and even undergo some elastic unloading immediately before failure. The first set of points is clearly located in the region of instability, and the second set of points is located in regions adjacent to the necking zone. This pattern is a characteristic of the process of strain localisation during the development of an instability.

The developed method is based on the physical description of the necking process presented previously to detect the onset of the plastic instability. The method is local and can therefore be applied to situations in which there is a non-negligible strain gradient through the thickness or along the sheet, e.g., in stretching processes with small-radius punches, stamping processes with high-curvature dies, etc.

For this purpose, the temporal evolution of the major strain (ε_1) and its first time derivative ($\dot{\varepsilon}_1$, major strain rate) are analysed for a series of aligned points on the exterior face of the sheet along a section perpendicular to the crack. Fig. 2 is a schematic of the time evolution of ε_1 and its time derivative $\dot{\varepsilon}_1$ at two representative points, A and B, in a section in the necking region.

The procedure is performed using the steps described below:

1. The width of the necking region is determined. As previously discussed, the strain of any point within this region increases until fracture occurs. The strain rate in the regions adjacent to the necking zone is gradually reduced until the strain rate evolution ceases, such that the points in these regions reach a constant level of strain or even undergo some elastic unloading before the sheet fractures. This behaviour can be observed at the limits of the necking region, which correspond to the last two points (marked with an A in Fig. 2) on either side of the crack that cease to strain and reach a zero strain rate just before the crack appears.

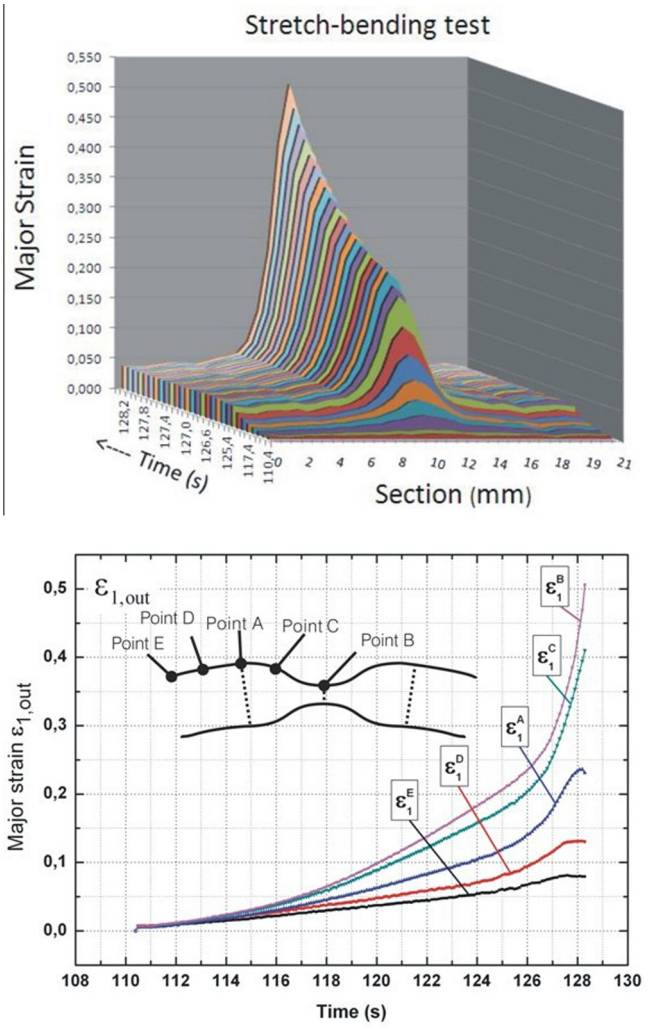

Fig. 1. Experimental time evolution of the major strain in a stretch-bending test with a Ø10mm cylindrical punch along a section perpendicular to the failure region (top) and at various aligned points from the same section (bottom).

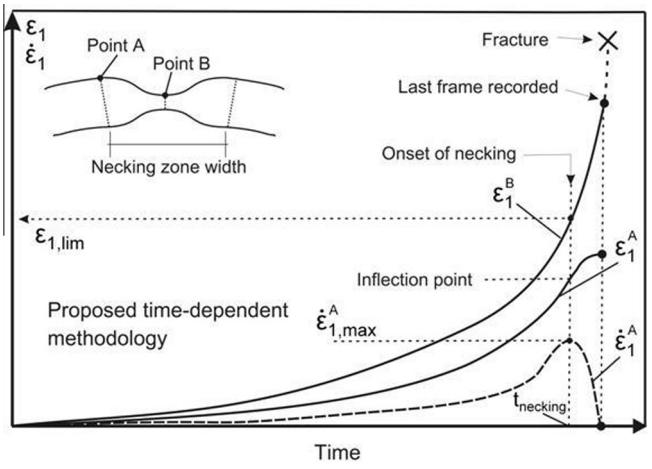

Fig. 2. Schematic of the developed time-dependent methodology.

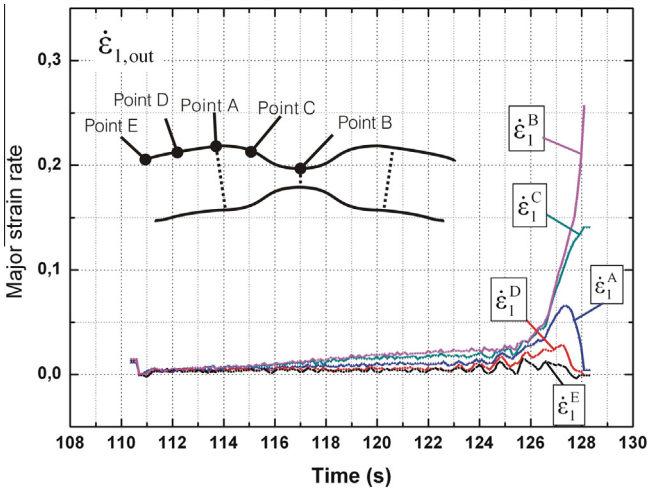

Fig. 3. Experimental evolution of the major strain rate in a test using a Ø10mm cylindrical punch.

Fig. 1 (bottom) and Fig. 3 show the experimental evolution of the major strain (ε_1) and its first time derivative ($\dot{\varepsilon}_1$) that corresponds to a stretch-bending test with a cylindrical punch of Ø10mm diameter. The differences in the evolutions of the points within and outside the necking region can be clearly identified in the figures.

2. The onset of necking is detected. Experimental evidence shows that the onset of necking is associated with a decreasing strain rate in the material adjacent to the necking region, vanishing before the fracture occurs. Therefore, the necking process begins when the strain rate at the boundary of the instability region (point A in Fig. 2) reaches a local maximum value ($\dot{\varepsilon}^{1,\max A}$). From this moment, denoted by $t_{necking}$ in Fig. 2, the strain rate at the limit of the necking region begins to decrease to zero, signalling the start of the strain localisation process inside the region.
3. The fracture initiation site is identified. The sheet fails at the point of greatest strain inside the necking region (point B in Fig. 2). The fracture point is identified as the point with a strain evolution curve above the strain curves for the other points in the necking region (ε_1^B in Fig. 2). By definition, the strain evolution of any point in the necking zone, and in particular that of point B, will always grow until failure.
   It should be noted that when a strain measurement system based on direct observation of the sheet surface is used, as will be seen below, the strain measured at the last frame captured by the system may likely underestimate the real fracture strain in the sheet, which should be obtained by direct measurement of the thickness strain after fracture. However, this does not affect the proposed method, since only a rough estimate of the time of failure is required for our purposes. And, in fact, this is captured with sufficient accuracy since the evolution of the strain at point B beyond the last frame recorded is a quasi-instantaneous process (see scheme in Fig. 2).
4. The major limit strain ($\varepsilon_{1,\text{lim}}$) is determined. This corresponds to the strain ε_1 at point B (ε_1^B) at the time of onset of the plastic instability, $t_{necking}$ (see Fig. 2).
5. The minor limit strain ($\varepsilon_{2,\text{lim}}$) is determined. This strain corresponds to the strain ε_2 at point B at the time $t_{necking}$.

Similarly to the ISO 12004-2:2008 [16], the method described above is applied to three adjacent sections perpendicular to the crack. The final limit strain is the average value of the strains determined in the three aforementioned sections. Henceforth, this method is referred to as the "t-d method" (time-dependent method).

Fig. 4. Hemispherical punch and specimens used in the Nakazima tests.

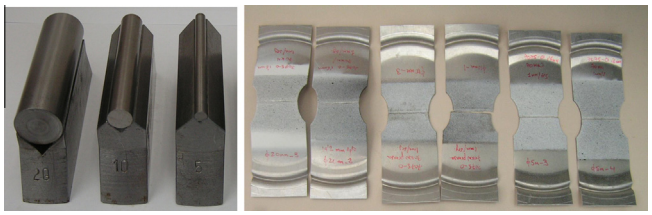

Fig. 5. Cylindrical punches and various test specimens used in the stretch-bending tests.

As previously shown, the developed method uses ε_1 as main analysis variable because this is directly measurable in the tests. However, from a physical perspective, the thickness strain ε_3 would appear to be a more appropriate analysis variable to detect the onset of necking because it directly quantifies the reduction in the thickness. Therefore, an alternative method based on a temporal analysis of ε_3 and its first time derivative can be proposed. The two methodologies will be compared later in the paper.

Finally, it should be noticed that a full determination of the conventional FLC using this methodology would require testing conditions, such as specimen geometry, strain paths, testing direction, lubrication systems and testing variables, similar to the specified in the ISO standard [16].

3. Experiments

A series of stretching and stretch-bending tests were conducted on 1.6-mm thick sheets of a 7075-O aluminium alloy. The samples were clamped at the edges and were strained until failure using punches with different geometries.

Two different experimental configurations were used. In one configuration, a series of Nakazima tests was conducted using a Ø100 mm hemispherical punch (see Fig. 4). In this case, three specimen geometries with different widths were used to obtain strain states approximating uniaxial tension, plane strain, and biaxial stretching (Fig. 4). In these assays, the strain was expected to be almost uniform throughout the thickness because of the generous radius of curvature of the punch, such that bending effects were negligible.

In the second configuration, a series of stretch-bending tests was conducted using cylindrical punches of Ø20, Ø10 and Ø5 mm (see Fig. 5). The geometry of the test pieces is also shown in Fig. 5. The width of these specimens was chosen such that approximate plane strain conditions were obtained in the failure region. Unlike the previous series of tests, this configuration introduces a significant strain gradient throughout the thickness in the failure region because of the simultaneous bending (due to the punch radius) and stretching actions.

An universal sheet metal testing machine, Erichsen, Model 142-20, was used to conduct the tests. The test pieces were clamped to the die with a blankholder force of 70 kN. A draw-bead was used to prevent slipping. The lubrication system between the

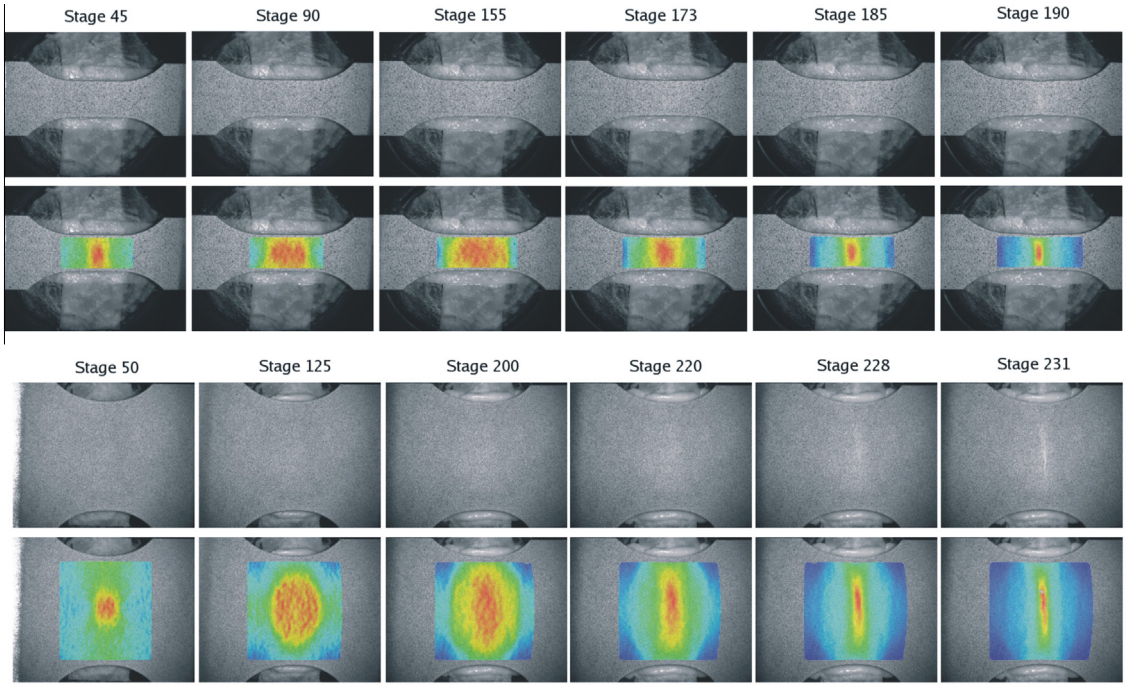

Fig. 6. Nakazima tests approximating uniaxial tension (top) and plane strain (bottom) during forming at different time steps (stages); images of the external sheet surface (upper images) and the contour map of the measured major strain (lower images).

punch and the sheet consisted of vaseline – PTFE – vaseline. Following the recommendations of ISO 12004-2:2008 [16], the punch speed was set at 1 mm/s in both series of tests. In each test, the strain was measured by optical methods and DIC techniques. The commercial software ARAMIS® was used in this calculation. The measurement procedure to evaluate the strain needed an initial high-contrast stochastic pattern of spots on the outer surface of the test piece. This pattern was created by spraying a background of flexible, adhesive, matte white paint on a previously degreased sheet (see specimens in Figs. 4 and 5). A customized paint was used, which resists up to 90–100% of true strain without deterioration. Later, a fine layer of spots of black paint was sprayed onto the background. During testing of the sheet until failure, the evolution of the spotted pattern was recorded using two 1.3 MPx digital CCD cameras at a rate of 10 images per second. The strain evaluation using the DIC method required the definition of a facet size, which depends on the pattern applied to the specimen surface, and a facet step, which defines the distance between two facet centre points. To optimise the CPU time while maintaining accuracy, a sensitivity study was performed to define the maximum facet size and step

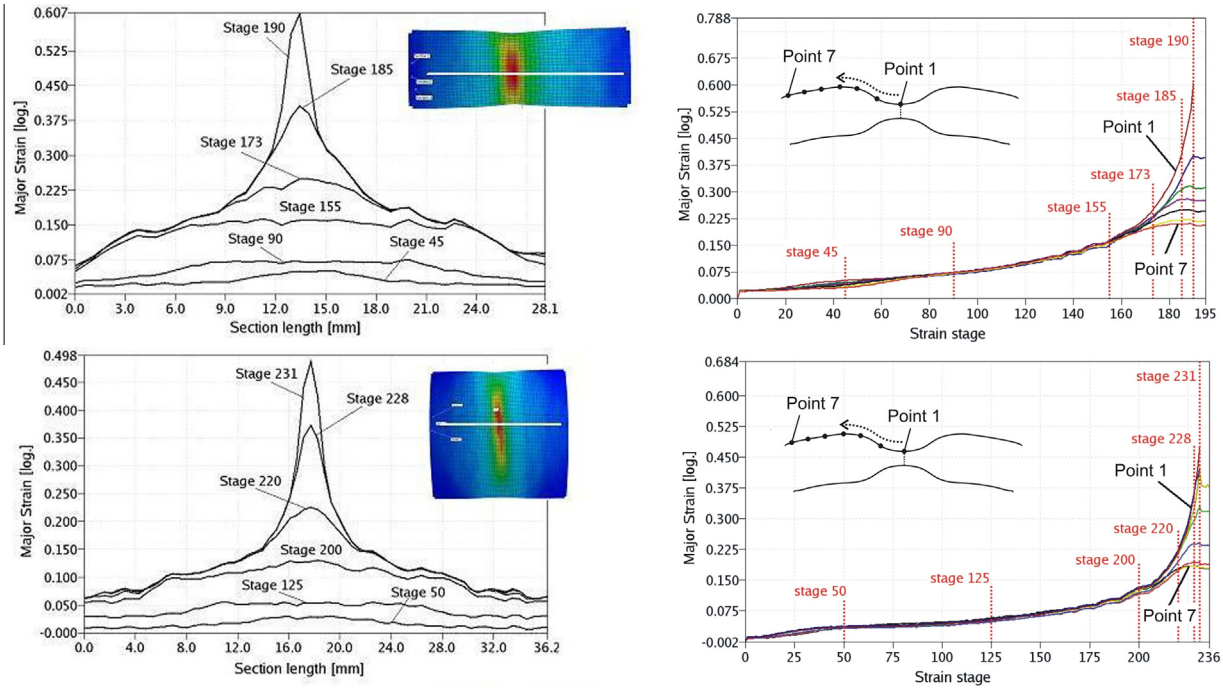

Fig. 7. Distribution of the major true strain along a given section line (left) and evolution of the major true strain versus the strain stage (time) at different section points (right) for Nakazima tests in uniaxial tension (top) and plane strain (bottom).

Table 1
Results for the Nakazima test close to plane strain conditions.

Test	ISO 12004-2:2008		T-d method ε_1		T-d method ε_3		Kitting et al.		Situ et al.		Situ et al., modified	
	ε_{1lim}	ε_{2lim}	ε_{1lim}	ε_{2lim}	ε_{1lim}	ε_{2lim}	ε_{1lim}	ε_{2lim}	ε_{1lim}	ε_{2lim}	ε_{1lim}	ε_{2lim}
I	0.274	−0.024	0.261	−0.026	0.261	−0.026	0.270	−0.018	0.324	−0.030	0.324	−0.030
II	0.231	−0.016	0.246	−0.019	0.246	−0.019	0.254	−0.018	0.305	−0.023	0.314	−0.024
III	0.245	−0.010	0.245	−0.012	0.245	−0.012	0.262	−0.013	0.305	−0.016	0.302	−0.015
IV	0.264	−0.021	0.255	−0.021	0.255	−0.021	0.273	−0.019	0.319	−0.027	0.319	−0.027
Mean	0.254	−0.018	0.252	−0.020	0.252	−0.020	0.265	−0.017	0.313	−0.024	0.315	−0.024
σ	0.019	0.006	0.008	0.006	0.008	0.006	0.009	0.003	0.010	0.006	0.009	0.007

Table 2
Results for the Nakazima test under approximate uniaxial tension conditions.

Test	ISO 12004-2:2008		T-d method ε_1		T-d method ε_3		Kitting et. al		Situ et al.		Situ et al., modified	
	ε_{1lim}	ε_{2lim}	ε_{1lim}	ε_{2lim}	ε_{1lim}	ε_{2lim}	ε_{1lim}	ε_{2lim}	ε_{1lim}	ε_{2lim}	ε_{1lim}	ε_{2lim}
I	0.323	−0.101	0.303	−0.101	0.306	−0.102	0.330	−0.086	0.422	−0.130	0.435	−0.128
II	0.314	−0.106	0.322	−0.103	0.322	−0.103	0.339	−0.102	0.425	−0.128	0.414	−0.118
III	0.346	−0.115	0.310	−0.100	0.319	−0.103	0.316	−0.099	0.514	−0.134	0.514	−0.134
Mean	0.328	−0.107	0.312	−0.101	0.316	−0.103	0.328	−0.096	0.454	−0.131	0.454	−0.127
σ	0.017	0.007	0.010	0.002	0.009	0.001	0.012	0.009	0.052	0.003	0.053	0.008

Table 3
Results for the Nakazima test under biaxial conditions.

Test	ISO 12004-2:2008		T-d method ε_1		T-d method ε_3		Kitting et al.		Situ et al.		Situ et al., modified	
	ε_{1lim}	ε_{2lim}	ε_{1lim}	ε_{2lim}	ε_{1lim}	ε_{2lim}	ε_{1lim}	ε_{2lim}	ε_{1lim}	ε_{2lim}	ε_{1lim}	ε_{2lim}
I	0.230	0.090	0.217	0.086	0.216	0.086	0.215	0.098	0.350	0.086	0.350	0.086
II	0.232	0.098	0.267	0.094	0.269	0.094	0.249	0.099	0.320	0.095	0.320	0.095
III	0.244	0.108	0.259	0.100	0.257	0.100	0.234	0.108	0.376	0.102	0.378	0.102
IV	0.246	0.080	0.242	0.082	0.235	0.081	0.230	0.080	0.340	0.080	0.355	0.080
V	0.219	0.081	0.244	0.077	0.243	0.077	0.248	0.084	0.358	0.079	0.364	0.078
VI	0.235	0.119	0.276	0.113	0.271	0.113	0.264	0.117	0.373	0.115	0.379	0.115
Mean	0.234	0.096	0.251	0.092	0.249	0.092	0.240	0.098	0.353	0.093	0.358	0.093
σ	0.010	0.015	0.021	0.013	0.021	0.013	0.017	0.014	0.021	0.014	0.022	0.014

Table 4
Results for Ø20 mm cylindrical punch tests.

Test	ISO 12004-2:2008		T-d method ε_1		T-d method ε_3		Kitting et. al		Situ et al.		Situ et al., modified	
	ε_{1lim}	ε_{2lim}	ε_{1lim}	ε_{2lim}	ε_{1lim}	ε_{2lim}	ε_{1lim}	ε_{2lim}	ε_{1lim}	ε_{2lim}	ε_{1lim}	ε_{2lim}
I	0.478	0.294	0.356	−0.022	0.356	−0.022	0.362	−0.016	0.425	−0.029	0.414	−0.029
II	0.239	0.201	0.298	−0.024	0.305	−0.024	0.294	−0.029	0.385	−0.024	0.371	−0.027
III	0.188	0.037	0.329	−0.028	0.328	−0.028	0.337	−0.021	0.406	−0.035	0.397	−0.037
Mean	0.302	0.177	0.328	−0.025	0.330	−0.025	0.331	−0.022	0.405	−0.029	0.394	−0.031
σ	0.155	0.130	0.029	0.003	0.026	0.003	0.034	0.007	0.020	0.006	0.022	0.005

Table 5
Results for Ø10 mm cylindrical punch tests.

Test	ISO 12004-2:2008		T-d method ε_1		T-d method ε_3		Kitting et. al		Situ et al.		Situ et al., modified	
	ε_{1lim}	ε_{2lim}	ε_{1lim}	ε_{2lim}	ε_{1lim}	ε_{2lim}	ε_{1lim}	ε_{2lim}	ε_{1lim}	ε_{2lim}	ε_{1lim}	ε_{2lim}
I	0.102	0.049	0.331	−0.008	0.331	−0.008	0.285	−0.012	0.411	−0.008	0.405	−0.007
II	0.442	0.268	0.356	−0.027	0.356	−0.027	0.300	−0.026	0.444	−0.022	0.444	−0.022
III	0.236	0.017	0.333	−0.025	0.332	−0.025	0.240	−0.020	0.431	−0.045	0.431	−0.045
Mean	0.260	0.111	0.340	−0.020	0.340	−0.020	0.275	−0.019	0.429	−0.025	0.427	−0.025
σ	0.171	0.137	0.014	0.010	0.014	0.010	0.031	0.007	0.017	0.019	0.020	0.019

Table 6
Results for Ø5 mm cylindrical punch tests.

Test	ISO 12004-2:2008		T-d method ε_1		T-d method ε_3		Kitting et. al		Situ et al.		Situ et al., modified	
	ε_{1lim}	ε_{2lim}	ε_{1lim}	ε_{2lim}	ε_{1lim}	ε_{2lim}	ε_{1lim}	ε_{2lim}	ε_{1lim}	ε_{2lim}	ε_{1lim}	ε_{2lim}
I	0.233	0.073	0.411	−0.043	0.416	−0.044	0.252	−0.039	0.539	−0.049	0.530	−0.050
II	0.442	0.041	0.430	−0.027	0.426	−0.027	0.244	−0.026	0.541	−0.014	–	–
III	0.279	−0.010	0.427	−0.047	0.430	−0.046	0.242	−0.033	0.490	−0.047	–	–
Mean	0.318	0.035	0.423	−0.039	0.424	−0.039	0.246	−0.033	0.523	−0.037	0.530	−0.050
σ	0.110	0.042	0.010	0.011	0.007	0.010	0.005	0.007	0.029	0.020	–	–

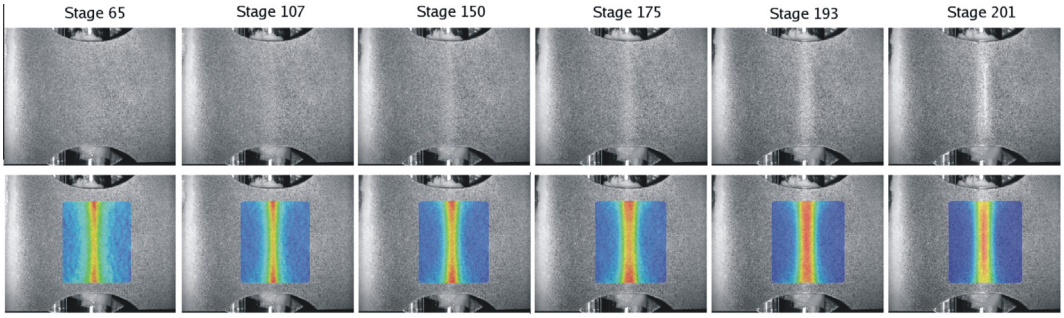

Fig. 8. Stretch-bending tests during forming with cylindrical punch of Ø20 mm at different time steps (stages): the upper images are of the external sheet surface and the lower images show contour maps of the measured major strain.

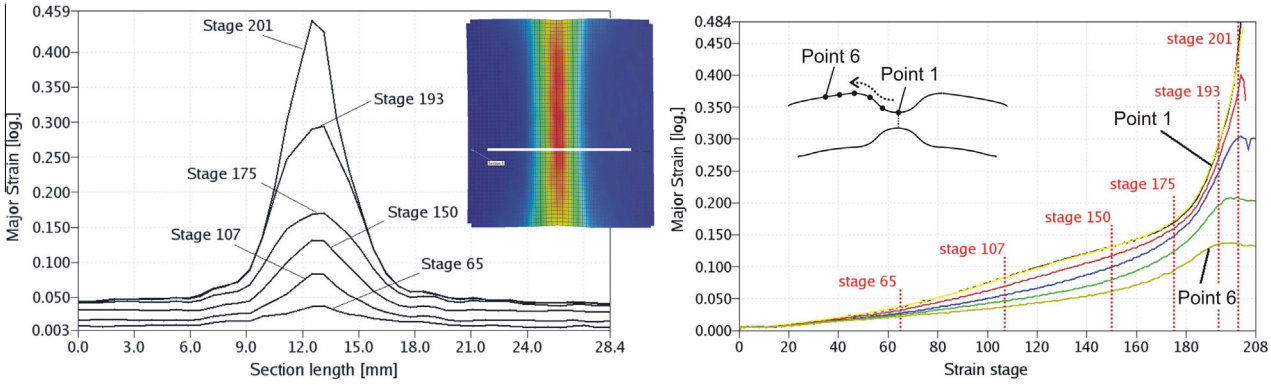

Fig. 9. Distribution of the major true strain along a given section line and evolution of the major true strain versus the strain stage (time) at different section points in a stretch-bending test with cylindrical punch of Ø20 mm.

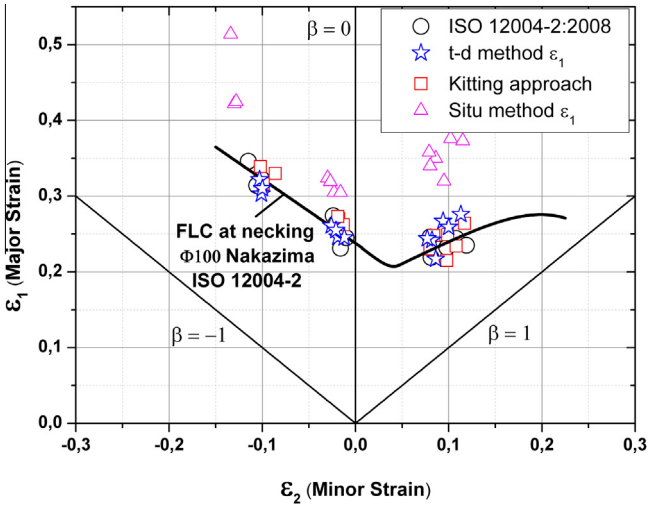

Fig. 10. Forming limit diagram (FLD) for several experimental methodologies and Nakazima tests for AA7075-O.

for each test configuration. A 13/11 (facet size/facet step) combination was used for the Nakazima tests. Ratios of 13/9, 13/7 and 11/7 were chosen for cylindrical punches of Ø20, 10 and 5 mm, respectively, in the stretch-bending tests.

4. Experimental results and comparative analysis

In this section, the experimental results obtained for both series of tests are presented, and the predictions of limit strains at the onset of necking using different criteria are analysed. Along with the ISO 12004-2:2008 method [16], used as a reference for Nakazima-type tests, the models by Situ et al. [21,22] and Kitting et al. [41] have been compared with the t-d method. These two models are local approaches, not originally restricted to the FLC assessment, and eventually applied to stretch-bending tests. A brief description of these two methods can be also found in [19].

The application of each of these criteria requires the measurement of the temporal and spatial evolution of the principal strains on the outer surface of the test piece in the vicinity of the failure region.

Fig. 6 shows the strain field on the outer sheet surface at different stages from the beginning of the process until the photogram (frame) prior to the ductile failure of the specimen for two different Nakazima tests. These data were obtained under experimental conditions approximating uniaxial tension (top) and plane strain (bottom). For these cases, Fig. 7 (left) shows the strain profile ε_1 along a section perpendicular to the failure region at the same stages. Such a section is shown on the ε_1 strain contour map at the frame immediately before the specimen fracture. The formation process of a localised neck was clearly distinguishable in all of the cases. In the early stages of the process, the strain was distributed approximately uniformly over the entire contact region between the punch and the sheet, while in the final stages, the strain was concentrated in a narrow band in which the sheet finally failed.

Fig. 7 (right) shows the temporal evolution of ε_1 for a series of points distributed from the fracture outward along the section shown in Fig. 7 (left). As mentioned before, the strain evolution at the different points practically superimposed during most of the test. The strain was only concentrated near the failure, where the curves dramatically separated from each other as a consequence of the development of the necking process.

Figs. 8 and 9 show the strain evolution in a stretch-bending test with cylindrical punch of Ø20 mm. Compared to the previous

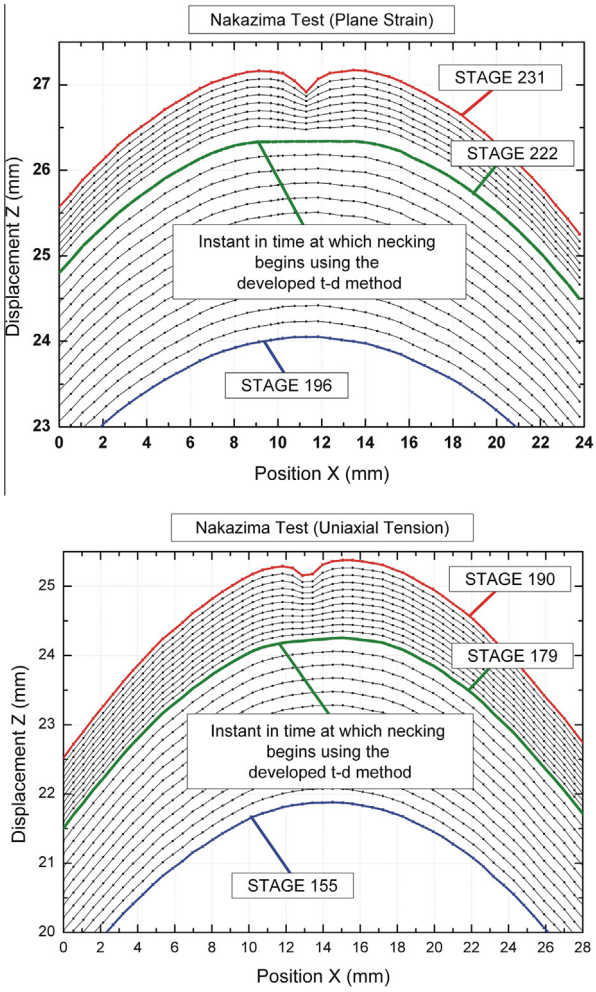

Fig. 11. Z-displacement along a perpendicular section to the failure region in the Nakazima tests under approximate plane strain conditions (top) and approximate uniaxial tension conditions (bottom).

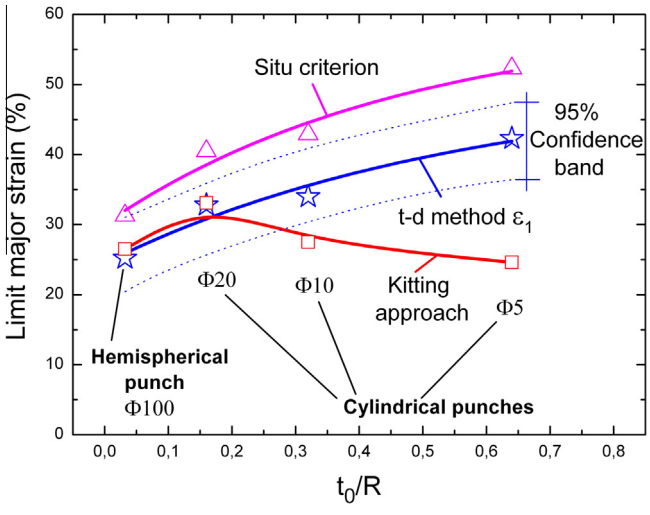

Fig. 12. Limit major strain evolution versus t_0/R using several methods near plane strain condition. The prediction band of 95% of confidence for t-d method is shown.

cases, a greater strain gradient was observed in the sheet, and the strain was concentrated over a smaller area because of the smaller radii of curvature of the punches. In the early stages of the test (see Fig. 9 left), the strains were highly localised in the central region,

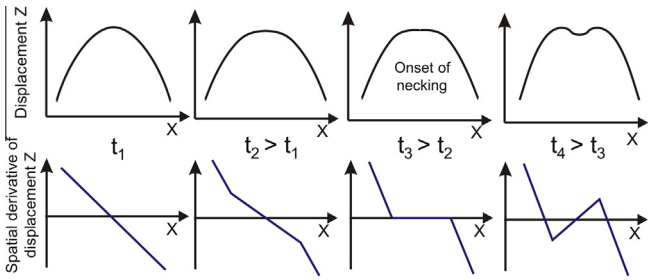

Fig. 13. Temporal evolution of the vertical displacement profile (top) and the spatial derivative (bottom) in a section perpendicular to the failure region.

exhibiting a dome-shaped spatial strain profile. In the subsequent stages of the test, the strains continued to localise until necking developed and sheet failure finally occurred.

Fig. 9 (right) shows the temporal evolution of ε_1 in a section perpendicular to the fracture region. The curves were substantially separated at the beginning of the test, unlike in the Nakazima tests (Fig. 7, right). This behaviour results from the strong strain gradient imposed by the punch along the sheet and across the sheet thickness. It can be seen that the severity of the gradient increased as the punch diameter decreased.

4.1. Nakazima test analysis

Tables 1–3 show the limit strains of the exterior face of the test piece for the Nakazima tests, which were estimated using the aforementioned methodologies. Following ISO 12004-2:2008 [16], each test result corresponded to the average of the values obtained for three different sections of the specimen, perpendicular to the fracture region. Four different specimens were tested for the plane strain case, three specimens were tested in uniaxial tension, and six specimens were tested under biaxial stretching. The mean value and the standard deviation (σ) are shown for each series of tests.

As mentioned before, the ISO 12004-2:2008 method [16] was designed and optimised for the conventional FLC, and therefore, its predictions have been taken here as reference values. These values are used to evaluate the capability of the other methodologies in estimating the limit strains for Nakazima tests.

As can be seen, the predictions of the two alternatives of the t-d method (using ε_1 and ε_3) were practically identical for all of the strain paths and very similar to those estimated by ISO 12004-2:2008 [16]. The maximum differences with the ISO method were in the 5% to 7% range. Similar results were obtained using the methodology of Kitting et al. [41]. However, the method of Situ et al. [21,22] and a modification of this method using ε_3 predicted substantially higher values than those obtained from ISO. All of the methodologies showed a remarkably small dispersion (as measured by the standard deviation).

Fig. 10 shows the FLC evaluated with ISO 12004-2:2008 [16] and the estimates obtained from the aforementioned methodologies. Only the results of the t-d method and the Situ criterion [21,22] based on ε_1 are shown for clarity. This figure and the previous tables show that both the developed t-d method and Kitting et al.'s [41] method adequately estimated the forming limits compared to the results obtained with the ISO. However, the temporal method developed here has the advantage of being a local method, which is independent of parameters or pre-defined fitting windows, unlike the ISO 12004-2:2008 [16]. Thus, this method can be directly applied to problems with non-negligible strain gradients. As we will show later, consistent results were not predicted by Kitting et al.'s method [41] in these cases.

A question naturally arises at this point of whether the t-d method adequately captures the onset of necking. Fig. 11 shows

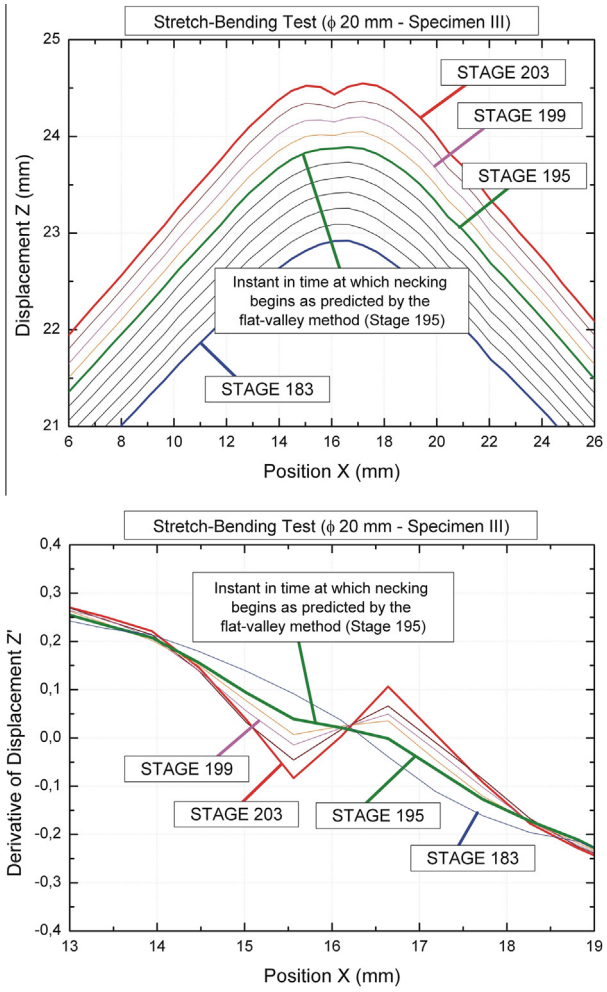

Fig. 14. Results for a stretch-bending test with cylindrical punch of Ø20 mm using the flat-valley method.

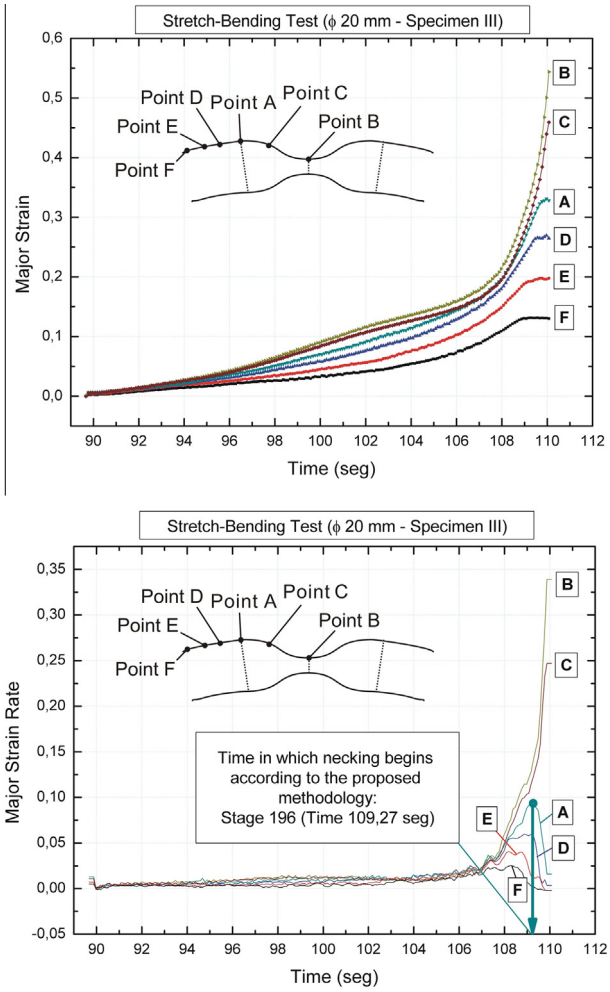

Fig. 15. Results for a stretch-bending test with cylindrical punch of Ø20 mm using the proposed t-d method.

Table 7
Results using the t-d and flat-valley methods for Ø20 mm cylindrical punch tests.

Test piece	Valley method		T-d method ε_1	
	ε_{1lim}	ε_{2lim}	ε_{1lim}	ε_{2lim}
I	0.314	−0.016	0.356	−0.022
II	0.282	−0.024	0.298	−0.024
III	0.337	−0.028	0.329	−0.028
Mean	0.311	−0.023	0.328	−0.025
σ	0.028	0.006	0.029	0.003

Table 8
Results using the t-d and flat-valley methods for Ø10 mm cylindrical punch tests.

Test piece	Valley method		T-d method ε_1	
	ε_{1lim}	ε_{2lim}	ε_{1lim}	ε_{2lim}
I	0.353	−0.008	0.331	−0.008
II	0.405	−0.030	0.356	−0.027
III	0.394	−0.027	0.333	−0.025
Mean	0.384	−0.022	0.340	−0.020
σ	0.027	0.012	0.014	0.010

the vertical displacement of the outer surface of the test piece along a section perpendicular to the failure region at different times until fracture. A plane strain and a uniaxial tension experiments are shown as examples. In agreement with the t-d method, necking started at stage 222 in the plane strain experiment and at stage 179 in the uniaxial tension experiment. Both times are identified in the figure. As can be seen, at earlier times, the outer surface profile evolves following the punch curvature; however, at later times, the profiles display a small valley or neck, which grows until the moment of fracture. At the exact moment of the onset of necking, the profiles are approximately flat, indicating that the sheet is not able to deform with the curvature imposed by the punch and pointing, therefore, the beginning of the plastic instability. As can be observed in Fig. 11, according to this description, the developed t-d method predicts the moment at which localised necking begin fairly precisely.

4.2. Stretch-bending test analysis

As in the previous section, Tables 4–6 show the predicted limit strains on the outer sheet face for the tests with the Ø20, Ø10, and Ø5 mm cylindrical punches, respectively. Three different samples were tested in each case.

Two significant observations called the applicability of ISO 12004-2:2008 [16] for these cases into question. First, the ISO predictions exhibited a large dispersion for the three cases, with a standard deviation on the order of the estimated average value. Second, positive ε_2 values were obtained for almost all of the cases, whereas the measured experimental strains ($\beta = \frac{\varepsilon_2}{\varepsilon_1}$) were always slightly negative. These results may be explained in terms of the size of the fitting windows used in the ISO method (see [19] for details), which were exceedingly large for these tests and led to

poorly conditioned inverse fitting parabolas. The dispersion for the other methodologies was substantially smaller than the average values. Again, no significant differences were observed between the predictions obtained with ε_1 or ε_3 for the developed t-d method. Similar behaviour was observed for the criterion of Situ et al. [21,22].

As we mentioned in the introduction, it is experimentally well established that bending causes the attainment of greater surface strains. This effect becomes more obvious as the severity of the strain gradient across the sheet thickness increases, e.g., with smaller punch radii [34–36,40,42]. This trend occurs while any indentation by the punch on the sheet is observed [43].

Fig. 12 plots the trend for the average value of the limit major strain (ε_1) on the outer face of the test piece versus the t_0/R ratio. This ratio indirectly quantifies the severity of the strain gradient [37]. The 95% confidence band for the t-d method is depicted. The confidence bands for the Kitting et al. [41] and Situ et al. [21,22] approaches are very similar to this, since the standard deviations are very much alike. These are omitted for clarity.

As can be seen the predictions from the method of Kitting et al. [41] did not exhibit an upward trend with increasing t_0/R, which was consistent with the aforementioned effect. Thus, the use of this method in tests with medium or small radii punches is highly questionable. However, the estimates obtained using the developed t-d method and the method of Situ et al. [21,22] exhibited the expected trend. As in the Nakazima tests, the method of Situ et al. [21,22] significantly overestimated the limit strain over the entire t_0/R range. Note some results are missing in Table 6. In these cases, the excessive noise in the second derivative of the strain prevented a reliable result from being obtained.

The results presented above show that the developed t-d method can consistently estimate limit strains in stretch-bending problems, for both smooth (e.g. Nakazima tests) and severe strain gradients (e.g. stretch-bending tests).

5. Direct observation of necking in stretch-bending: the flat-valley method

As we previously discussed for the Nakazima tests, the predictions of the developed t-d method for the onset of necking were validated by analysing the displacement of the outer surface of the test piece over the duration of the test. This evolution allowed the onset of necking to be directly observed, which was associated with the appearance and development of a valley in the profile. This method for identifying the necking process can be an alternative method (to previously used methods) in itself. The appearance of this valley has been also observed by Li et al. [28] to corroborate the localised necking in AA5182-O.

Fig. 13 is a schematic of the displacement perpendicular to the plane of the non-deformed test piece (Z axis) for a section perpendicular to the failure region at different times (t_1 denotes a time far from necking and t_4 denotes a time just before fracture). As can be seen, for times far from the failure (i.e., t_1 in Fig. 13), the surface of the test piece deforms by adequately conforming to the curvature imposed by the cylindrical punch. However, the curve begins to flatten in a localised region at t_2 and becomes flat at t_3 until finally a necking valley is observed at t_4.

The outer geometry begins to flatten because the thickness of the central region reduces more rapidly than at adjacent points. When the profile becomes flat, the test piece simultaneously begins to deform independently of the curvature imposed by the punch. This event physically corresponds to the onset of necking ($t_{necking} = t_3$ in Fig. 13). At subsequent times, the valley in the test piece geometry can be clearly seen and progressively deepens until the sheet fractures.

This flattening process, which is accompanied by the subsequent onset of the necking valley, is more easily identified by calculating the first spatial derivative of the vertical Z displacement (see Fig. 13, bottom). The onset of necking corresponds graphically to a local change in the slope at the strain localisation region relative to the slope of the neighbouring points. The plastic instability occurs in this manner when the slope remains constant, that is, when the curve becomes flat. Analogously to the procedure shown in Fig. 2, the limit strain $\varepsilon_{1,\mathrm{lim}}$ is obtained at the time $t_{necking}$ on the curve corresponding to the point at which fracture is initiated.

This physical process of strain localisation is independent of the test type. This method can be classified as a hybrid method that depends on both time and position because it involves the time evolution of the outer test piece geometry in a section perpendicular to the failure region to identify the onset of necking and estimate the limit strains. Henceforth, this method will be referred to as the "flat-valley method".

Fig. 14 shows the experimentally measured displacement at the exterior sheet surface and its spatial derivative at different times (stages) for test III of the Ø20 mm cylindrical punch. The instant at which necking began according to the valley method is highlighted in green in the same figure (stage 195). Note that the spatial derivative of the displacement profile showed a greater flatness at these times and that a sign change was observed in the next time instant. Given the discrete nature of the experimental curves, the greater the number of photograms taken, the more accurately can the time at which a constant slope occurs be captured in practice.

Fig. 15 shows the trends in the major strains and their time derivatives at different points along a section perpendicular to the crack for the same test. The instant in time at which the developed t-d method predicted the onset of necking is indicated (stage 196). This prediction almost coincided with the flat-valley method (stage 195), yielding both method similar limit strains, as shown in Tables 7 and 8.

As can be seen, the flat-valley method adequately reproduced the aforementioned experimental trend, and the limit strains increased with the severity of the bending. The dispersion of the predictions was also small. However, the most noteworthy result was that the predictions of both methods agreed reasonably with each other. The maximum deviations oscillated approximately 5–10% around the average values.

In summary, this study shows that both the t-d method and the flat-valley method predict similar forming limit strains, which are consistent with the experimental evidence. Both methods adequately reproduce the physical phenomena associated with the onset of necking and the subsequent development of localised necking. The onset of necking estimated by direct observation, using the flat-valley method, allowed to validate the results obtained with the t-d method for cases with negligible strain gradients (Nakazima tests) and strong strain gradients (stretch-bending tests).

6. Conclusions

In this article, two physically-based methodologies, categorized as a time-dependent method (t-d method) and a time-position-dependent method (so called here flat-valley method), have been described and analysed in detail to assess the failure by necking.

A series of Nakazima and stretch-bending tests for different punch radii were performed on an AA7075-O alloy of 1.6mm thickness to evaluate the capabilities of the developed methodologies and other methods reported in the literature. The commercial software ARAMIS® was used to measure and compute the displacement and strain evolutions at the outer surface of the tested specimens along a section perpendicular to the crack.

The main findings can be outlined as follows:

1. In the t-d method, the onset of necking was detected by the appearance of a maximum in the first time derivative of ε_1 at the boundary of the instability region. This region of instability, or necking region, included all points that increased monotonically their level of strain until fracture occurred.
2. In the flat-valley method, the initiation of necking was inferred when the slope in the first spatial derivative of the vertical displacement remained constant within the necking region. This corresponded with a flattening in the displacement curve, as a consequence of the onset of the local plastic instability.
3. Both methodologies successfully predicted the necking limit strains in stretch-bending tests, where the strain gradient across the sheet thickness was considerable at the initiation of necking.
4. The methods by Kitting et al. and Situ et al., and particularly the method by ISO 12004-2:2008, specially designed for the FLC determination, failed in their estimates when they were applied to these situations.
5. For the Nakazima tests, the proposed methods satisfactorily matched the results given by ISO 12004-2:2008, becoming in an appealing alternative for the determination of the FLC.

In summary, the two developed methodologies successfully estimated the onset of necking and the limit strains in sheet-forming under significant through-thickness strain gradients. The local character of these methods enables its application independent of the type of test performed, e.g. Nakazima tests, stretch-bending tests, etc.

Acknowledgements

The authors wish to express their gratitude to DGICyT of Spain for funding this research within the framework of projects DPI2009-13335 and DPI2012-32913.

References

[1] Hill R. On discontinuous plastic states, with special reference to localized necking in thin sheets. J Mech Phys Solids 1952;1(1):19–30.
[2] Swift HW. Plastic instability under plane stress. J Mech Phys Solids 1952;1(1):1–18.
[3] Marciniak Z, Kuczynski K. Limit strains in processes of stretch-forming sheet metal. Int J Mech Sci 1967;9(9):609–20.
[4] Hutchinson JW, Neale KW. Sheet necking-II. Time-independent behaviour. In: Koistinen DP, Wang NM, editors. Mechanics of sheet metal forming. Plenum; 1978. p. 127–53.
[5] Eyckens P, Van Bael A, Van Houtte P. Marciniak-Kuczynski type modelling of the effect of through-thickness shear on the forming limits of sheet metal. Int J Plast 2009;25:2249–68.
[6] Eyckens P, Van Bael A, Van Houtte P. An extended Marciniak-Kuczynski model for anisotropic sheet subjected to monotonic strain paths with through-thickness shear. Int J Plast 2011;27:1577–97.
[7] Zadpoor AA, Sinke J, Benedictus R. Formability prediction of high strength aluminium sheets. Int J Plast 2009;25:2269–97.
[8] Zadpoor AA, Campoli A, Sinke J, Benedictus R. Fracture in bending – the straining limits of monolithic sheets and machined tailor-made blanks. Mater Des 2011;32(3):1229–41.
[9] Zhang L, Wang J. Modeling the localized necking in anisotropic sheet metals. Int J Plast 2012;39:103–18.
[10] Firat M. A finite element modeling and prediction of stamping formability of a dual-phase steel in cup drawing. Mater Des 2012;34:32–9.
[11] Bragard A, Baret JC, Bonnarens H. A simplified method to determine the FLD onset of localized necking. Rapport Centre de Recherche de la Metallurgie 1972;33:53–63.
[12] D'Haeyer R, Bragard A. Determination of the limiting strains at the onset of necking. Rapport Centre de Recherche de la Metallurgie 1975;42:33–5.
[13] Vacher P, Haddad A, Arrieux R. Determination of the forming limit diagrams using image analysis by the correlation method. CIRP Ann Manuf Technol 1999;48(1):227–30.
[14] Sène NA, Balland P, Arrieux R. About necking detection to determine forming limit diagrams for mini stamping. In: Proc. 17th international scientific and technical conference, design and technology of drawpieces and die stampings, Poland. 2008, p. 241–53.
[15] Sène NA, Balland P, Arrieux R, Bouabdalah K. An experimental study of the microformability of very thin materials. Exp Mech 2012;53(2):155–62.
[16] International Standard ISO 12004-2:2008. Metallic materials-sheet and strip-determination of forming limit curves, Part 2: Determination of forming limit curves in the laboratory. International Organization for Standardization, Geneva, Switzerland; 2008.
[17] Hotz W, Timm J. Experimental determination of forming limit curves (FLC). In: Hora P, editor. Proc. of the 7th numisheet conference and workshop, Interlaken, Switzerland. 2008, p. 271–8.
[18] Martínez-Donaire AJ, Vallellano C, Morales D, García-Lomas FJ. On the experimental detection of necking in stretch-bending tests. Am Inst Phys Conf Proc 2009;1181:500–8.
[19] Martínez-Donaire AJ, Vallellano C, Morales D, García-Lomas FJ. Experimental detection of necking in stretch-bending conditions: a critical review and new methodology. Steel Res Int 2010;81(9 suppl):785–8.
[20] Geiger M, Merklein M. Determination of forming limits diagrams-a new analysis method for characterization of materials' formability. CIRP Ann Manuf Technol 2003;52(1):213–6.
[21] Situ Q, Jain M, Bruhis M. A suitable criterion for precise determination of incipient necking in sheet materials. Mater Sci Forum 2006;519–521:111–6.
[22] Situ Q, Jain MK, Bruhis M. Further experimental verification of a proposed localized necking criterion. In: Proc. Numerical Methods in Industrial Forming Processes – 9th Numiform, Porto, Portugal. 2007, p. 907–12.
[23] Situ Q, Jain MK, Bruhis M, Metzger DR. Determination of forming limit diagrams of sheet materials with a hybrid experimental–numerical approach. Int J Mech Sci 2011;53:707–19.
[24] Eberle B, Volk W, Hora P. Automatic approach in the evaluation of the experimental FLC with a full 2D approach based on a time depending method. In: Hora P, editor. Proc. of the 7th numisheet conference and workshop, Interlaken, Switzerland. 2008, p. 279–84.
[25] Feldmann P, Schatz M, Aswendt P. Automatic FLC-value determination from 4D strain data. In: Proc. International Deep Drawing Research Group IDDRG, Golden, USA. 2009, p. 533–46.
[26] Volk W, Hora P. New algorithm for a robust user-independent evaluation of beginning instability for the experimental FLC determination. Int J Mater Form 2010;4:339–46.
[27] Merklein M, Kuppert A, Geiger M. Time dependent determination of forming limit diagrams. CIRP Ann Manuf Technol 2010;59:295–8.
[28] Li J, Carsley JE, Stoughton TB, Hector LG, Hu SJ. Forming limit analysis for two-stage forming of 5182-O aluminum sheet with intermediate annealing. Int J Plas 2013;45:21–43.
[29] Hotz W, Merklein M, Kuppert A, Friebe H, Klein M. Time dependent FLC determination – comparison of different algorithms to detect the onset of unstable necking before fracture. Key Eng Mater 2013;549:397–404.
[30] Merklein M, HuBnatter W, Geiger M. Characterization of yielding behaviour of sheet metal under biaxial stress condition at elevated temperature. CIRP Ann Manuf Technol 2008;57:269–74.
[31] Leppin C, Li J, Daniel D. Application of a method to correct the effect of non-proportional strain paths on Nakajima test based forming limit curves. In: Hora P, editor. Proc. of the 7th numisheet conference and workshop, Interlaken, Switzerland. 2008, p. 217–21.
[32] Ghosh AK, Hecker SS. Stretching limits in sheet metals: in-plane versus out-of-plane deformation. Metall Trans 1974;5:2161–4.
[33] Charpentier PL. Influence of punch curvature on the stretching limits of sheet steel. Metall Trans A 1975;6(9):1665–9.
[34] Tharret MR, Stoughton TB. Stretch-bend forming limits of 1008 AK steel. Society of Automotive Engineers, SAE Paper No. 2003-01-1157; 2003.
[35] Tharrett MR, Stoughton TB. Stretch-bend forming limits of 1008 AK steel, 70/30 brass, and 6010 aluminum. In: Khan AS, Kazmi R, Zhou J, editors. Dislocations, plasticity and metal forming: proc. of the 10th international symposium on plasticity and its current applications, Quebec, Canada. p. 199–201.
[36] Atzema EH, Fictorie E, van den Boogaard AH, Droog JMM. The influence of curvature on FLC's of mild steel, (A)HSS and aluminium. In: Proc. International Deep Drawing Research Group IDDRG, Graz, Austria. 2010, p. 519–28.
[37] Col A, Balan T. About the neglected influence of gradients on strain localisation. In: Proc. Numerical Methods in Industrial Forming Processes – 9th Numiform, Porto, Portugal. 2007, p. 147–52.
[38] Kitting D, Koplenig M, Ofenheimer A, Pauli H, Till ET. Application of a "Concave-Side Rule" approach for assessing formability of stretch-bent steel sheets. Int J Mater Form 2009;2(Suppl. 1):427–30.
[39] Morales D, Martínez-Donaire AJ, Vallellano C, García-Lomas FJ. Bending effect in the failure of stretch-bend metal sheets. Int J Mater Form 2009;2:813–6.
[40] Morales D, Vallellano C, García-Lomas FJ. Assessment of the effect of the through-thickness strain/stress gradient on the formability of stretch-bend metal sheets. Mater Des 2013;50:798–809.
[41] Kitting D, Ofenheimer A, Pauli H, Till ET. Forming limits of stretch-bent steel sheets. In: Proc. international deep drawing research group IDDRG, Golden, USA. p. 425–35.
[42] Fictorie E, van den Boogaard AH, Atzema EH. Influence of punch radius in a Nakazima test for mild steel and aluminium. Int J Mater Form 2010;3(suppl. 1):1179–82.
[43] Martínez-Donaire AJ. Análisis del efecto del gradiente de deformaciones en el conformado de chapa metálica. PhD dissertation. Spain: University of Seville; 2012.